Clays and Clay Minerals, Vol. 46, No. 5, 574–582, 1998.

SURFACE MICROTOPOGRAPHY OF LATH-SHAPED HYDROTHERMAL ILLITE BY TAPPING-MODE™ AND CONTACT-MODE AFM

YOSHIHIRO KUWAHARA,[1] SEIICHIRO UEHARA[2] AND YOSHIKAZU AOKI[2]

[1] Department of Evolution of Earth Environments, Graduate School of Social and Cultural Studies, Kyushu University, Ropponmatsu, Fukuoka 810, Japan

[2] Department of Earth and Planetary Sciences, Faculty of Science, Kyushu University, Hakozaki, Fukuoka 812, Japan

Abstract—Lath-shaped hydrothermal illite particles in Izumiyama pottery stone were examined by contact-mode atomic force microscopy (CMAFM) and tapping-mode AFM (TMAFM) in air. With CMAFM, the lath-shaped particles showed interlacing patterns on the (001) surface in deflection images, while in height images such patterns were unclear. Also, evidence of artifacts caused by frictional forces between the surface and tip and/or edge effects were found in the CMAFM height images of the particle and Si substrate surfaces. In contrast, TMAFM showed interlacing patterns clearly in both amplitude and height images, and artifacts were barely evident. The TMAFM height images permitted the accurate measurement of 1.0- or 2.0-nm height steps corresponding to single or double mica layers, as well.

Many lath-shaped particles in the Izumiyama hydrothermal illite exhibit interlacing patterns on their (001) surface, as shown by these AFM observations. The interlacing patterns are characterized by polygonal spirals with comparatively wide spacings and steps having a height of 1.0 or 2.0 nm. Generally a single lath-shaped particle has a single spiral center on the (001) surface, and 2 mica layers rotated 120° originate from the dislocation point. These support the view that lath-shaped illites belong to the $2M_1$ polytype. It is likely that these illite particles were formed by a uniform process of development that is characterized by very slow growth, spiral mechanisms in that growth and low supersaturation conditions.

Key Words—Contact-Mode AFM, Hydrothermal Illite, Interlacing Pattern, Microtopography, Polytype, Spiral Growth, Tapping-Mode AFM.

INTRODUCTION

AFM produces microtopographic images and surface atomic resolution images of both conductors and nonconductors (Binnig et al. 1986). Samples can be imaged in air, in solutions or in a vacuum. At present, several different scanning methods in AFM have been used to study surface microtopography and the atomic-scale structure of various materials (for example, CMAFM, TMAFM, noncontact-mode AFM). CMAFM, in which the scanning tip gently touches the sample surface, has produced many significant surface images of clay and sheet silicate minerals under ambient conditions (chlorite—Wicks et al. 1993; Vrdoljak et al. 1994, goethite—Weidler et al. 1996; illite—Hartmann et al. 1990; Blum 1994; Nagy 1994; illite–smectite—Lindgreen et al. 1991; Blum 1994; kaolinite—Kumai et al. 1995; lizardite—Wicks et al. 1992; Wicks et al. 1993; and muscovite—Wicks et al. 1993; Blum 1994). However, in CMAFM in air the frictional forces between the tip and surface cause substantial damage to both sample and tip and create artifacts in the image data (Drake et al. 1989; Eggleston 1994).

This problem has largely been overcome by techniques (for example, CMAFM in liquids, TMAFM) that reduce the tip force applied to the sample. CMAFM in liquids has been a promising tool for imaging biological samples without significant disruption of the biological structure (Butt et al. 1990; Durbin and Carlson 1992; Hansma et al. 1992; Mazzola and Fodor 1995), and its high lateral resolution has allowed the production of excellent atomic resolution images of mineral surfaces (Drake et al. 1989; Weisenhorn et al. 1990; Johnsson et al. 1991; Rachlin et al. 1992; Ohnesorge and Binnig 1993; Stipp et al. 1994; Wicks et al. 1994). The dissolution and growth processes of minerals in solutions have also been observed in real time by means of CMAFM in liquids (Gratz et al. 1991, 1992; Hillner et al. 1992; Dove and Hochella 1993; Dove and Chermak 1994; Maurice et al. 1994). However, AFM observation of ultrafine particles such as clay minerals in solutions has been rare because of the difficulty posed in fixation of samples on the substrate in solutions. Only recently has this problem been overcome to a limited extent using TMAFM in fluid (Bickmore and Hochella 1997).

TMAFM is a technique developed by Digital Instruments in 1992, and has been recently used to obtain high resolution topographic images of soft and fragile samples in both air (Umemura et al. 1993; Zhong et al. 1993; Gref et al. 1994; Huber et al. 1994) and liquids (Putman et al. 1994; Radmacher et al. 1994; Hansma et al. 1995; Grantham and Dove 1996). TMAFM is operated by oscillating the cantilever assembly at or near the cantilever's resonant frequency using a piezoelectric crystal. In contrast to CMAFM, it has sufficient oscillation amplitude to overcome the

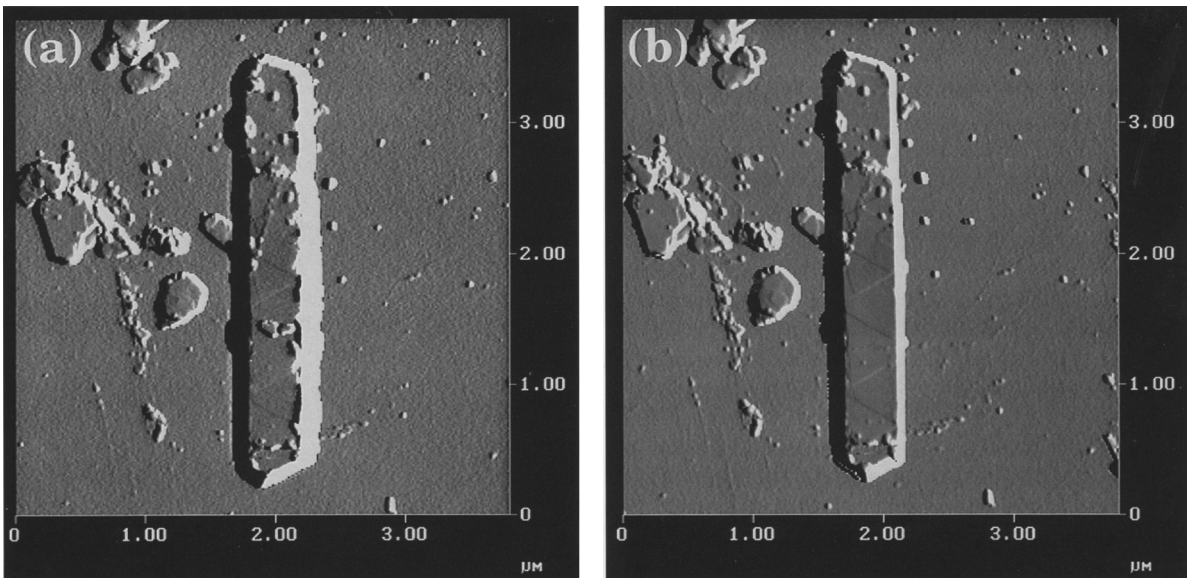

Figure 1. CMAFM deflection (a) and TMAFM amplitude (b) images of a lath-shaped particle at 1 Hz.

tip-sample adhesion forces when the tip contacts the surface. Also, the surface material is not pulled sideways by shear forces, since the applied force is always vertical (Digital Instruments 1993; Grantham and Dove 1996).

In the present study, the authors compared TMAFM with conventional CMAFM, noting in particular the accuracy of 3-dimensional data of clay size particles under ambient conditions. Clearer microtopographic images and more accurate height information of lath-shaped illite particles were obtained by TMAFM. Furthermore, the results showed that many lath-shaped Izumiyama hydrothermal illite particles belong to the $2M_1$ polytype. This is inconsistent with a previous conclusion (Inoue et al. 1987, 1988; Baronnet 1992) that lath-shaped and platy illites have typically $1M$ and $2M_1$ structures, respectively, which was reached as a result of studies that used transmission electron microscopy (TEM) and X-ray powder diffraction (XRD).

MATERIALS AND METHODS

Hydrothermal illite (Sample IZ2, Hirasawa and Uehara 1998) in the Izumiyama pottery stone from Arita, Saga Prefecture, Japan, was used in this study. The XRD pattern of the sample shows that illite polytypes are mainly $2M_1$ and $2M_2$ with minor amounts of $1M$ (Hirasawa and Uehara 1998).

A Si wafer, polished perfectly flat at the subnanometer scale, was used as the mounting material for AFM observation. A drop of a dilute suspension of illite in distilled water was evaporated onto a Si wafer.

The AFM used was a Nanoscope III with a Multimode SPM unit (Digital Instruments, Inc.). Samples were examined first by TMAFM and then by CMAFM. The images were all taken in air using a J-head piezoelectric scanner (about 125 μm *XY* scans and 5 μm *Z* scan). A J-head piezo scanner is favorable for finding some suitable particles from abundant particles by means of its wider *XY* scan ranges, although one is inferior to an A- or E-head piezo scanner in resolution. Cantilevers used in our experiments were 200-μm, wedge-shaped Si_3N_4 units with a force constant of 0.12 N/m in CMAFM, and 125-μm-long Si cantilevers with a force constant of 20–100 N/m in TMAFM. The scanning rate was 1.0 Hz to 4.0 Hz. Setpoint voltages and integral and proportional gains were adjusted for each scan as appropriate. We collected parallel height and deflection images in CMAFM and height and amplitude images in TMAFM. The height image is digitally recorded surface topography. The deflection and amplitude images are essentially a record of the error in the height image of the sample under a constant force mode and serve to amplify the stepped appearance on the surface.

RESULTS AND DISCUSSION

Comparison between CMAFM and TMAFM Images

The CMAFM deflection and TMAFM amplitude images of a lath-shaped hydrothermal illite particle at 1 Hz are shown in Figure 1. Interlacing patterns can be seen on the (001) surface of the particle in both the deflection and amplitude images. However, interlacing patterns are much clearer in the amplitude image. The sides, especially the right side, of the lath-shaped particle are steeper in the amplitude image than in the deflection image.

https://doi.org/10.1346/CCMN.1998.0460511 Published online by Cambridge University Press

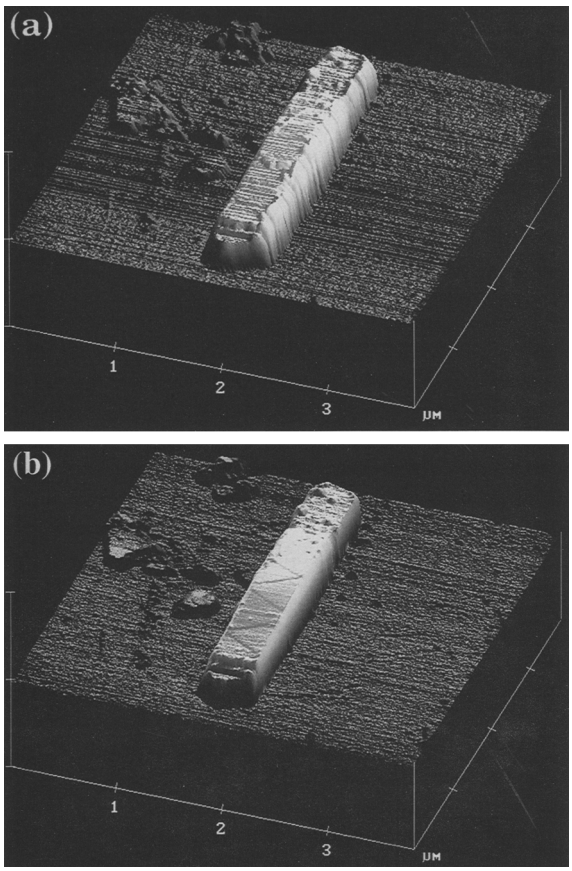

Figure 2. Height images of lath-shaped particle by both CMAFM (a) and TMAFM (b) at 1 Hz; Z = 200 nm. Artifactual stripes parallel to the scanning direction are observed in (a). The steps as can be seen in (b) have a height of 1.0 nm.

Figure 2 presents another comparison of CMAFM and TMAFM. Here we see the height images of the lath-shaped particle at 1 Hz. These 3-dimensional images are processed by adding an illumination-effect to the original height images in order to show the surface microtopography more clearly. The length, width and thickness of the particle are 3.13 μm, 0.39 μm and 186 nm, respectively, in both CMAFM and TMAFM images. In the CMAFM height image (Figure 2a), interlacing patterns, which are seen in the deflection image, are unclear. Instead, artifactual stripes parallel to the scanning direction are clearly observed on the Si substrate surface and the (001) surface of illite as if the surfaces were scratched by the scanning tip. These artifacts are created by high frictional forces between the tip and the surface (Drake et al. 1989; Eggleston 1994). We should be careful not to overlook these artifacts because the stripes were barely visible in both the deflection images and the original height images prior to the application of illumination-weighting. At 4 Hz in CMAFM, other stripes perpendicular to the stripes that are parallel to the scanning direction were observed on the Si substrate along the right-hand edge of the image. This is the "edge-effect" occurs when the feedback electronics which attempt to keep either the force or height constant are imperfect, particularly in high-resolution imaging or at a higher scanning rate (Eggleston 1994).

In the TMAFM height image (Figure 2b), interlacing patterns are visible on the (001) surface of the lath-shaped particle, as can be seen in the amplitude image (Figure 1b). The individual steps have a height of 1.0 nm, which corresponds to thickness of a single mica layer. The step spacings are 450–550 nm. The artifactual stripes shown in CMAFM were hardly observed in TMAFM, even at 4 Hz.

The sides of the lath-shaped particle shown in the TMAFM height images are steeper than those in the CMAFM height images, as can be seen also in the deflection and amplitude images. These are artifacts that reflect the shape of the scanner tip. A Si_3N_4 cantilever used in CMAFM has a pyramid-shaped tip with a solid angle of 70°, whereas a Si cantilever for TMAFM has a sharper tip with a solid angle of 35°. When the tip scans over any topographic feature that is steeper than the taper angle of the tip, the point of the tip will lose contact with the surface as the side of the tip rides over the edge of the feature (Eggleston 1994). Therefore, the result is an image that mirrors the side shape of the tip.

Figure 3 is a cross-sectional view and a height histogram of the data points within the box showing a single mica layer step, from height images of both CMAFM and TMAFM using a J-head piezo scanner. In CMAFM, the step structure is unclear due to the artifactual stripes (Figures 3a and 3c) and, therefore, the step height cannot be measured. A cross-sectional view (Figure 3d) along the white line in Figure 3b collected by TMAFM illustrates that the step has a height of 1.0 nm and both mica layers across the step are nearly flat. Figure 3f shows that we can get accurate height information from the TMAFM images, even on the order of a unit cell. This height histogram (Figure 3f) obtained from a TMAFM image has higher

→

Figure 3. a) and b) Close-up views of the lower end of the particle in Figures 2a (by CMAFM) and 2b (by TMAFM), respectively. c) and d) Cross-sectional views along the white lines in (a) and (b), respectively. e) and f) Height histograms of the data points within the box in (a) and (b), respectively.

https://doi.org/10.1346/CCMN.1998.0460511 Published online by Cambridge University Press

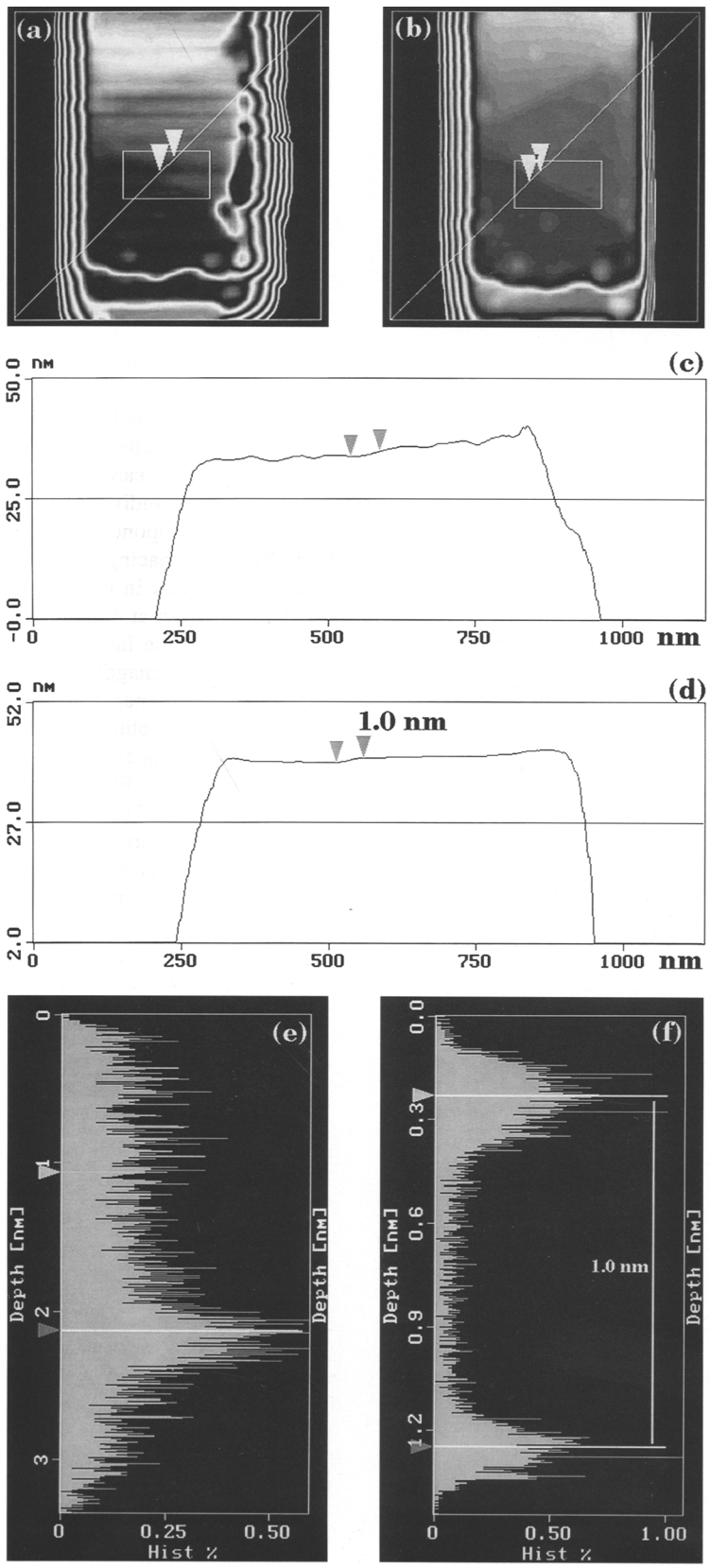

https://doi.org/10.1346/CCMN.1998.0460511 Published online by Cambridge University Press

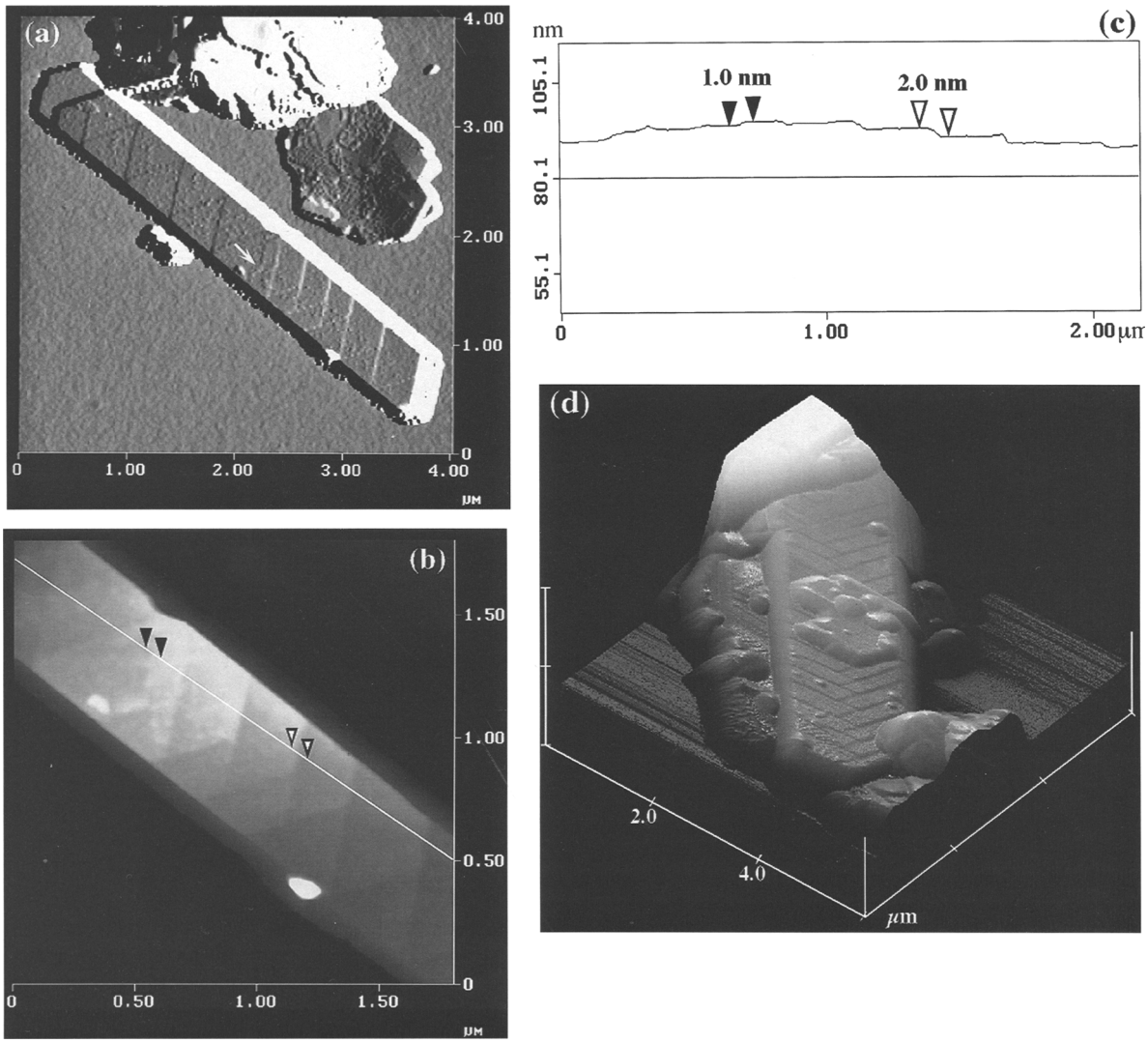

Figure 4. a) TMAFM amplitude image showing representative interlacing patterns observed on the basal plane of a lath-shaped particle. The step heights are 1.0 nm in the zigzag step pattern areas and 2.0 nm in parallel step areas. White arrow indicates a dislocation point generating 120° rotation of double mica layers. b) TMAFM height image enlarged a central part of (a); Z = 300 nm. c) A cross-sectional view along the white line in (b). Black and white pointers correspond to those in (b). d) TMAFM height image showing interlacing patterns on wider lath-shaped particle surface; Z = 600 nm.

resolution than a height histogram showing a 1-nm step on the muscovite surface obtained from a CMAFM image in Figure 2 of Blum (1994). Therefore, TMAFM is a good choice for the microtopographic imaging and analysis of clay particles.

Interlacing Patterns on the (001) Surface of Lath-Shaped Izumiyama Hydrothermal Illite

Figure 4a shows representative interlacing patterns observed on the (001) surface of a lath-shaped Izumiyama hydrothermal illite. The particle is higher in the middle and lower at its ends, so the pattern is likely the manifestation of a growth spiral elevated at its center (Figures 4b and 4c). The spiral center on the central part of the particle exhibits 2 mica layers rotated 120° from each other, which originate from the dislocation point. Very clear, uniform zigzag patterns are evident on the left-hand surface of the particle. The steps have a height of 1.0 nm, and the step separations are 400–500 nm. On the right-hand surface of the particle, the spacings between successive steps are narrower than those on the left hand surface (150–350 nm), widening from the center to the end of the particle. Zigzag patterns of 1.0 nm steps are observed only on the central area along the length of the lath-shaped particle. Parallel steps stretched to both sides of the zigzag areas

https://doi.org/10.1346/CCMN.1998.0460511 Published online by Cambridge University Press

have a height of 2.0 nm corresponding to double mica layers height (Figures 4b and 4c). This different step height between the left- and right-hand surfaces of the particle was caused by the anisotropy of advancing step rates and the 120° rotation of 2 mica layers, as described below.

Figure 4d shows interlacing patterns observed on the (001) surface of a wider lath-shaped illite. The step spacings are as wide as those on the right-hand surface of the illite particle in Figure 4a (200–350 nm). Many lath-shaped Izumiyama illite particles have approximately the same step spacings. Therefore, on the surface of wider lath-shaped illite, parallel step areas tend to be larger than zigzag step areas, whereas more slender lath-shaped particles develop zigzag step patterns on the surfaces.

An interlacing pattern is not expected in minerals, such as kaolinite, that exhibit 1-layer stacking (Sunagawa and Koshino 1975). Only simple 1-layer spirals or their derivatives are seen on their surfaces. On the other hand, the TEM decoration technique reveals that dickite, nacrite and $2M$ micas that exhibit 2-layer stacking have interlacing patterns on their basal planes (Sunagawa and Koshino 1975; Tomura et al. 1976; Kitagawa et al. 1983).

Figure 5 illustrates interlacing patterns expected for the case presented in this paper. Here, 2 identical elongated hexagonal spiral layers rotated 120° originate from a single dislocation point. The upper layer overtakes the lower layer at the sides of the hexagonal. The lath-shaped particle is elongated to an extreme degree in a diagonal direction ([100]) of a hexagonal by the anisotropy of crystal face growth rates (Figures 4a and 5). Zigzag pattern areas develop in the diagonal direction of the hexagonal and parallel steps stretch to both sides of the zigzag areas. Since many lath-shaped Izumiyama hydrothermal illite particles show such interlacing patterns on their surfaces (Figures 1 and 4), all these particles must belong to the $2M_1$ polytype.

The interlacing patterns on the lath-shaped illite surfaces are characterized by the development of polygonal spirals with 150–550 nm step separations. These step separations are as wide as those of the other hydrothermal illite reported by Kitagawa et al. (1983). They suggested that hydrothermal illite that exhibits such spirals is grown in a hydrothermal metasomatic environment in which original solid rocks are dissolved to form low supersaturated solutions instead of directly from hydrothermal solution. Illite precipitated directly from hydrothermal solution exhibits circular spirals with narrower step separations (Sunagawa and Koshino 1975; Kitagawa et al. 1983). In the present AFM observation, circular spirals or others supporting a $1M$ polytype were not observed on the (001) surfaces of any lath-shaped particles.

Inoue et al. (1988) showed that the growth of illitic minerals during smectite-to-illite conversion in the hydrothermal setting consists of 2 distinct growth sequences: One is the growth of lath-shaped particles present in illite–smectite (I–S) with 55–20% expandable layers, continuing metastably up to 0% expandable layers. The second stage is the growth of hexagonal particles in I–S with 20–0% expandable layers. The first stage corresponds to the evolution from $1Md$ to $1M$ illite. The second stage corresponds to the evolution of $2M_1$ illite.

Lath-shaped Izumiyama illite particles exhibit interlacing patterns on their surfaces, suggesting a $2M_1$ polytype. In addition, this illite sample (IZ2) contains less than 5% expandable layers (Hirasawa and Uehara 1998). Therefore, lath-shaped particles of Izumiyama hydrothermal illite were probably formed very slowly under low supersaturation conditions, without passing through smectite-to-illite conversion. This process is consistent with the growth sequence of the hexagonal particles of Inoue et al. (1988) rather than the lath-shaped particles. Hence, there may be no correlation between the morphology and polytype of hydrothermal illite. Rather, polytypes and spiral shapes of hydrothermal illite are likely controlled by the supersaturation condition of the solution, as described by Baronnet (1992).

But it has been found by our AFM experiments until now that Izumiyama hydrothermal illite particles consist not only of lath-shaped, but also platy (circular, rectangular, hexagonal and other polygonal) forms. The lath-shaped particles belong to a $2M_1$ polytype, whereas platy particles have a $1M$ or $2M_1$ polytype. Also differences both in particle thickness and in step spacing have been found between the lath-shaped and platy particles. This information would be helpful for understanding growth mechanism of Izumiyama hydrothermal illite. The AFM study of the morphology, microtopography and polytype of their particles is now underway.

CONCLUSIONS

This study demonstrated that, in air, TMAFM is extremely useful for the microtopographic observation and analysis of clay particles. Although both the CMAFM deflection and the TMAFM amplitude images were able to capture interlacing patterns on the (001) surfaces of the particles, the interlacing patterns were observed more clearly in the TMAFM amplitude images. In the CMAFM height images, interlacing patterns on the surface were unclear due to artifactual stripes caused by high frictional forces between the tip and the surface and/or by edge effect. In contrast to this, the TMAFM height images showed interlacing step patterns clearly on the particle surface, and the artifacts as shown in CMAFM images were barely evident in TMAFM images, even at a faster scanning rate. Indeed, not only were the interlacing steps clearly visible in the TMAFM height images, but the step

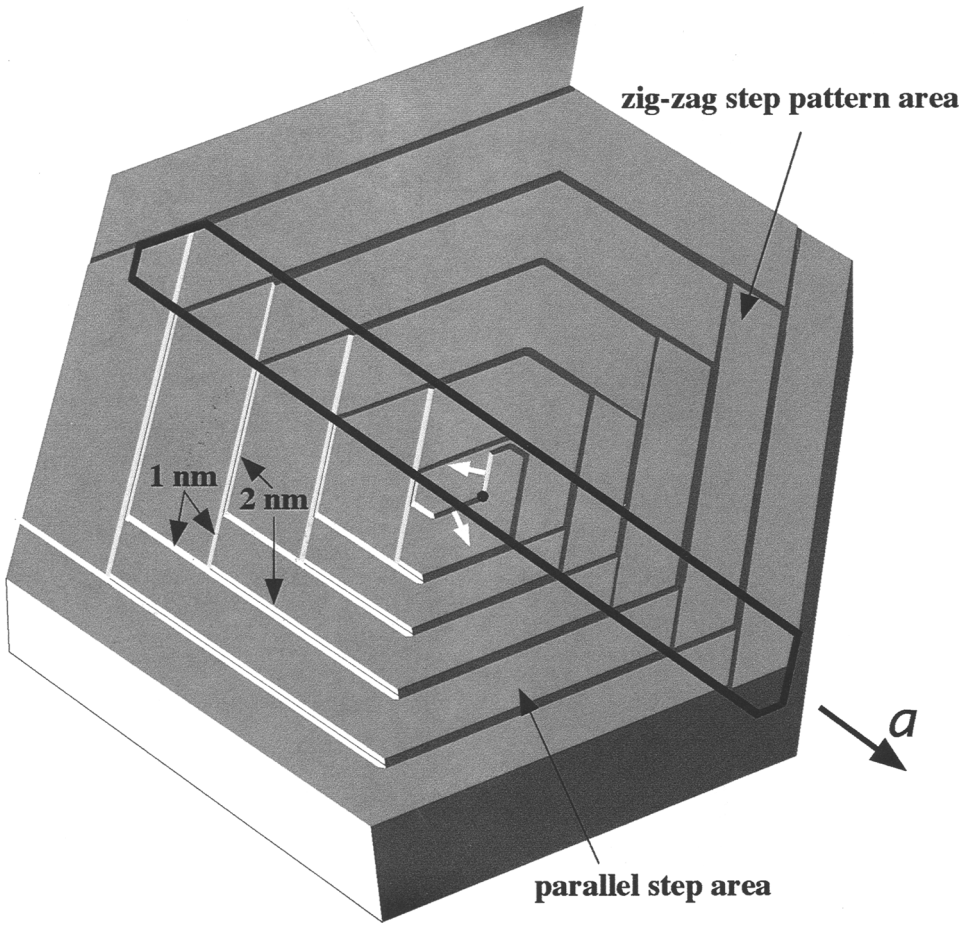

Figure 5. Schematic drawing of spiral growth of an illite particle and interlacing patterns expected for the present case in which 2 hexagonal spiral layers rotated 120° originate from a single dislocation point. The lath-shaped form surrounded by bold solid lines corresponds to that of the illite particle in Figure 4a. The lath-shaped particle elongates in the [100] direction. A point in a central part of the particle shows the single dislocation point. Two white arrows indicate the 2 spiral directions.

heights could be accurately measured as either 1.0 nm or 2.0 nm, corresponding to single or double mica layers, respectively.

It was confirmed by the present TMAFM observations that many lath-shaped particles in Izumiyama hydrothermal illite exhibit interlacing patterns that are characterized by polygonal spirals with relatively wide spacings on their (001) surface. The lath-shaped particles belong to the $2M_1$ polytype. They were formed very slowly under lower supersaturation conditions by spiral growth mechanisms.

ACKNOWLEDGMENTS

We are grateful to I. Sinno, H. Sakai and Y. Nakamuta of Kyushu University for helpful suggestions. We also extend heartfelt thanks to K. Ishida of Kyushu University for his careful review of this manuscript. The authors thank 2 reviewers, K. L. Nagy of Sandia National Laboratories and B. R. Bickmore of Virginia Tech, for helpful and constructive reviews. This study was supported in part by the Grant-in-Aid for Scientific Research (No. 06402021) from Ministry of Education of Japan.

REFERENCES

Baronnet A. 1992. Polytypism and stacking disorder. In: Buseck PR, editor. Minerals and reactions at the atomic scale: Transmission electron microscopy. Rev Mineral 27. Washington, DC: Mineral Soc Am. p 231–288.

Bickmore BR, Hochella MF Jr. 1997. The particle specific nature of mica weathering: Real-time observation of K^+ exchange in clay-sized mica particles using fluid cell TMAFM™. In: 7th Ann VM Goldschmidt Conf; LPI Contribution No. 921, Lunar and Planetary Institute, Houston. p 27–28.

Binnig G, Quate CF, Gerber Ch. 1986. Atomic force microscope. Phys Rev Lett 56:930–933.

Blum AE. 1994. Determination of illite/smectite particle morphology using scanning force microscopy. In: Nagy KL, Blum AE, editors. Scanning probe microscopy of clay minerals. CMS workshop lectures, vol 7. Boulder, CO: Clay Miner Soc. p 172–202.

Butt H-J, Wolff EK, Gould SAC, Dixon Northern B, Peterson CM, Hansma PK. 1990. Imaging cells with the atomic force microscope. J Struct Biol 105:54–61.

Digital Instruments. 1993. Nanoscope III Comand reference manual Vers. 3.0. Santa Barbara, CA 93103: Digital Instruments Inc. 227 p.

Dove PM, Hochella MF Jr. 1993. Calcite precipitation mechanisms and inhibition by orthophosphate: *In situ* observations by scanning force microscopy. Geochim Cosmochim Acta 57:705–714.

Dove PM, Chermak JA. 1994. Mineral-water interactions: Fluid cell applications of scanning force microscopy. In: Nagy KL, Blum AE, editors. Scanning probe microscopy of clay minerals. CMS workshop lectures, vol 7. Boulder, CO: Clay Miner Soc. p 140–169.

Drake B, Prater CB, Weisenhorn AL, Gould SAC, Albrecht TR, Quate CF, Cannell DS, Hansma HG, Hansma PK. 1989. Imaging crystals, polymers, and processes in water with the atomic force microscope. Science 243:1586–1589.

Durbin SD, Carlson WE. 1992. Lysozyme crystal growth studied by atomic force microscopy. J Crystal Growth 122: 71–79.

Eggleston CM. 1994. High-resolution scanning probe microscopy: Tip-surface interaction, artifacts, and applications in mineralogy and geochemistry. In: Nagy KL, Blum AE, editors. Scanning probe microscopy of clay minerals. CMS workshop lectures vol. 7. Boulder, CO: Clay Miner Soc. p 3–90.

Grantham MC, Dove PM. 1996. Investigation of bacterial-mineral interactions using fluid tapping mode™ atomic force microscopy. Geochim Cosmochim Acta 57:2473–2480.

Gratz AJ, Manne S, Hansma PK. 1991. Atomic force microscopy of atomic-scale ledges and etch pits formed during dissolution of quartz. Science 251:1343–1346.

Gratz AJ, Hillner PE, Hansma PK. 1992. Step dynamics and spiral growth on calcite. Geochim Cosmochim Acta 57: 491–495.

Gref R, Minamitake Y, Peracchia MT, Trubetskoy V, Torchilin V, Langer R. 1994. Biodegradable long-circulating polymeric nanospheres. Science 263:1600–1603.

Hansma HG, Vesenka J, Siegerist C, Kelderman G, Morrett H, Sinsheimer RL, Elings V, Bustamante C, Hansma PK. 1992. Reproducible imaging and dissection of plasmid DNA under liquid with the atomic force microscope. Science 256:1180–1184.

Hansma HG, Laney DE, Bezanilla M, Sinsheimer RL, Hansma PK. 1995. Applications for atomic force microscopy of DNA. Biophys J 68:1672–1677.

Hartmann H, Sposito G, Yang A, Manne S, Gould SAC, Hansma PK. 1990. Molecular-scale imaging of clay mineral surfaces with the atomic force microscope. Clays Clay Miner 38:337–342.

Hillner PE, Gratz AJ, Manne S, Hansma PK. 1992. Atomic-scale imaging of calcite growth and dissolution in real time. Geology 20:359–362.

Hirasawa K, Uehara S. 1998. Microtexture and microstructure of illite from the Izumiyama pottery stone, Arita, Saga Prefecture. In: A study of mineral boundary and surface by HRTEM and AFM. Progress Report of a Grant-in-Aid for Scientific Research (C) from the Ministry of Education, Science, Sports and Culture. Project No. 07640645. p 14–33 (in Japanese).

Huber CA, Huber TE, Sadoqi M, Lubin JA, Manalis S, Prater CB. 1994. Nanowire array composites. Science 263:800–802.

Inoue A, Kohyama N, Kitagawa R, Watanabe T. 1987. Chemical and morphological evidence for the conversion of smectite to illite. Clays Clay Miner 35:111–120.

Inoue A, Velde B, Meunier A, Touchard G. 1988. Mechanism of illite formation during smectite-to-illite conversion in a hydrothermal system. Am Mineral 73:1325–1334.

Johnsson PA, Eggleston CM, Hochella MF Jr. 1991. Imaging molecular-scale structure and microtopography of hematite with the atomic force microscope. Am Mineral 76:1442–1445.

Kitagawa R, Takeno S, Sunagawa I. 1983. Surface microtopographies of sericite crystals formed in different environmental conditions. Mineral J 11:282–296.

Kumai K, Tsuchiya K, Nakato T, Sugahara Y, Kuroda K. 1995. AFM observation of kaolinite surface using "pressed" powder. Clay Sci 9:311–316.

Lindgreen H, Garnæs J, Hansen PL, Besenbacher F, Lægsgaard E, Stensgaard I, Gould SAC, Hansma PK. 1991. Ultrafine particles of North Sea illite/smectite clay minerals investigated by STM and AFM. Am Mineral 76:1218–1222.

Maurice PA, Hochella MF Jr, Parks GA, Sposito G, Schwertmann U. 1994. Evolution of hematite surface microtopography upon dissolution by simple organic acids. Clays Clay Miner 43:39–50.

Mazzola LT, Fodor SPA. 1995. Imaging biomolecule arrays by atomic force microscopy. Biophys J 68:1653–1660.

Nagy KL. 1994. Application of morphological data obtained using scanning force microscopy to quantification of fibrous illite growth rates. In: Nagy KL, Blum AE, editors. Scanning probe microscopy of clay minerals. CMS workshop lectures, vol 7. Boulder, CO: Clay Miner Soc. p 204–239.

Ohnesorge F, Binnig G. 1993. True atomic resolution by atomic force microscopy through repulsive and attractive forces. Science 260:1451–1456.

Putman CAJ, van der Werf KO, de Grooth BG, van Hulst NF, Greve J. 1994. Viscoelasticity of living cells allows high resolution imaging by tapping mode atomic force microscopy. Biophys J 67:1749–1753.

Rachlin AL, Henderson GS, Goh MC. 1992. An atomic force microscope (AFM) study of the calcite cleavage plane: Image averaging in Fourier space. Am Mineral 77:904–910.

Radmacher M, Fritz M, Hansma HG, Hansma PK. 1994. Direct observation of enzyme activity with the atomic force microscope. Science 265:1577–1579.

Stipp SLS, Eggleston CM, Nielsen BS. 1994. Calcite surface structure observed at microtopographic and molecular scales with atomic force microscopy (AFM). Geochim Cosmochim Acta 58:3023–3033.

Sunagawa I, Koshino Y. 1975. Growth spirals on kaolin group minerals. Am Mineral 60:407–412.

Tomura S, Kitamura M, Sunagawa I. 1976. Surface microtopography of metamorphic white micas. Phys Chem Miner 5:65–81.

Umemura K, Arakawa H, Ikai A. 1993. High resolution images of cell surface using a tapping mode atomic force microscope. Japan J Appl Phys 32:L1711–L1714.

Vrdoljak GA, Henderson GS, Fawcett JJ. 1994. Structural relaxation of the chlorite surface imaged by the atomic force microscope. Am Mineral 79:107–112.

Weidler PG, Schwinn T, Gaub HE. 1996. Vicinal faces on synthetic goethite observed by atomic force microscopy. Clays Clay Miner 44:437–442.

Weisenhorn AL, Mac Dougall JE, Gould SAC, Cox SD, Wise WS, Massie J, Maivald P, Elings B, Stucky GD, Hansma PK. 1990. Imaging and manipulating molecules on a zeolite surface with an atomic force microscope. Science 247: 1330–1333.

Wicks FJ, Kjoller K, Henderson GS. 1992. Imaging the hydroxyl surface of lizardite at atomic resolution with the atomic force microscope. Can Mineral 30:83–91.

Wicks FJ, Kjoller K, Eby RK, Hawthorne FC, Henderson GS, Vrdoljak GA. 1993. Imaging the internal atomic structure of layer silicates using the atomic force microscope. Can Mineral 31:541–550.

Wicks FJ, Henderson GS, Vrdoljak GA. 1994. Atomic and molecular scale imaging of layered and other mineral structures. In: Nagy KL, Blum AE, editors. Scanning probe microscopy of clay minerals. CMS workshop lectures, vol 7. Boulder, CO: Clay Miner Soc. p 92–138.

Zhong Q, Inniss D, Kjoller K, Elings VB. 1993. Fractured polymer/silica fiber surface studied by tapping mode atomic force microscopy. Surface Sci Lett 290:L688–L692.

(Received 6 August 1997; accepted 6 March 1998; Ms. 97-072)